energies

MDPI

Article

# A DC Microgrid Coordinated Control Strategy Based on Integrator Current-Sharing

**Liyuan Gao [1,*], Yao Liu [2], Huisong Ren [1] and Josep M. Guerrero [3]**

1 Department of Electrical Engineering, Shandong University, Jinan 250061, China; 18763572405@163.com
2 Zhuhai Power Supply Bureau of Guangdong Power Grid Corporation, Zhuhai 519000, China; yaoliu@csu.edu.cn
3 Department of Energy Technology, Aalborg University, DK-9220 Aalborg East, Denmark; joz@et.aau.dk
* Correspondence: 17853125839@163.com

Received: 10 July 2017; Accepted: 25 July 2017; Published: 1 August 2017

**Abstract:** The DC microgrid has become a new trend for microgrid study with the advantages of high reliability, simple control and low losses. With regard to the drawbacks of the traditional droop control strategies, an improved DC droop control strategy based on integrator current-sharing is introduced. In the strategy, the principle of eliminating deviation through an integrator is used, constructing the current-sharing term in order to make the power-sharing between different distributed generation (DG) units uniform and reasonable, which can reduce the circulating current between DG units. Furthermore, at the system coordinated control level, a hierarchical/droop control strategy based on the DC bus voltage is proposed. In the strategy, the operation modes of the AC main network and micro-sources are determined through detecting the DC voltage variation, which can ensure the power balance of the DC microgrid under different operating conditions. Meanwhile, communication is not needed between different DG units, while each DG unit needs to sample the DC bus voltage, which retains the plug-and-play feature of the DC microgrid. The proposed control strategy is validated by simulation on a DC microgrid with permanent magnet synchronous generator-based wind turbines, solar arrays and energy storage batteries, which can be applied to small commercial or residential buildings.

**Keywords:** DC microgrid; DC bus voltage; hierarchical/droop control strategy; current-sharing; power balance

## 1. Introduction

Distributed generation (DG) is becoming a complementary to and a support of future large power grids due to the advantages of low pollution, high energy utilization efficiency, flexible installation location, low transmission and distribution resources loss and low electric transmission line loss. For these reasons, DG is increasingly cited as a key feature of future power systems [1,2]. Microgrids, an effective carrier of distributed generation resources (DGR), consist of various DG units, energy storage devices, energy conversion devices, protection devices and load control devices. Being able to operate in islanded and grid-connected modes, microgrids have become an effective way for DGR integration in recent years [3,4].

However, the power supply quality of microgrids is influenced by the intermittence and fluctuation of distributed micro-power to some extent. Moreover, some alternating current (AC) distributed power sources are connected to the microgrid through a multi-stage conversion, which lowers microgrid efficiency. Establishing direct current (DC) transmission lines in microgrids to connect a number of DGRs and the energy storage (ES) system to form a DC microgrid can allow for better coordination and control of DGRs, so as to improve power supply quality and decrease the

impact on the AC main network [5–11]. Hence, technologies relevant to DC microgrids have attracted extensive attention in the research community.

The earliest studies on the structure and control methods of DC power networks originated from DC nanogrids [12–17]. Bryan et al. [12] proposed using DC bus voltage as the control signal, differentiating operation modes by the value of DC bus voltage, which is allowed to change in a certain range; however, the grid-connected mode was not taken into account. In [18,19], more complicated operation conditions were considered, but the control strategy could only be applied to particular DC microgrid structures, thus limiting its universality. Therefore, in-depth discussion on micro-source control strategies under different working modes needs to be made so as to ensure the reliability of DC microgrids.

At present, the major control strategies to maintain power balance in DC microgrids are centralized control [20] and decentralized control [21–23]. In centralized control, a central controller is used to execute instructions to the micro-source unit to maintain power balance in the system. However, this requires a fast communication bandwidth, and a single communication failure can disrupt proper DC microgrid operations. To solve these problems, a droop control strategy based on conventional synchronous generator characteristics was introduced in [21–23]. The power balanced state of a DC microgrid can be judged according to the changing DC bus voltage since it is the trigger sign of power balance. However, without working in the maximum power point tracking (MPPT) mode, the output characteristics of micro-sources were not taken into consideration in the conventional droop control strategy, thereby lowering the energy utilization efficiency of the system. In order to solve this problem, an ES unit was used to overcome the output fluctuation and randomness of micro-sources in [24–29], which can reduce the frequent fluctuations of the DC bus voltage and enhance system stability [7–11].

In this paper, by taking advantage of conventional control strategies, a hierarchical/droop control strategy based on DC bus voltage is proposed, which can ensure that different DGs cooperate to provide power, making the system operate in the optimum state and the microgrid bus voltage maintained in a reasonable range. The operation modes of the AC main network and controllable micro-sources are determined through detecting DC bus voltage change, so as to ensure the power balance of the DC microgrid when the DC bus voltage is in a different hierarchical range. Taking into full consideration the actual output characteristics of micro-sources, the proposed strategy can overcome the fluctuations through the ES unit and engage micro-sources in MPPT mode as much as possible to enhance the system efficiency. Moreover, the flexibility and reliability are enhanced while the system cost is reduced since no communication between different units is needed, making the system a plug-and-play solution. Finally, a simulation model is built with a wind turbine (WT)/photovoltaic (PV)/ES DC microgrid as the paradigm, which can be applied to different scenarios, such as small-sized commercial and residential buildings. Simulation results have verified the effectiveness and feasibility of the introduced strategy for a DC microgrid operating in different modes.

The rest of the paper is organized as follows. Section 2 starts with the structure of the DC microgrid based on PV, WT and ES, and then, the operation modes of each unit and the mode-switching process are introduced. In Section 3, the control strategies at the converter level, as well as in system level are presented. Simulation results with the control strategies are shown and discussed in Section 4. Finally, Section 5 presents the conclusions.

## 2. DC Microgrid Structure and Composition

### *2.1. DC Microgrid Structure*

The configuration of the DC microgrid studied in this paper is shown in Figure 1. The photovoltaic array, wind turbine generator and storage battery are connected through a DC-DC converter or AC-DC converter to form the DC microgrid. The microgrid is linked with the AC main network by a bilateral converter, while the AC and DC loads obtain electric power from the DC bus.

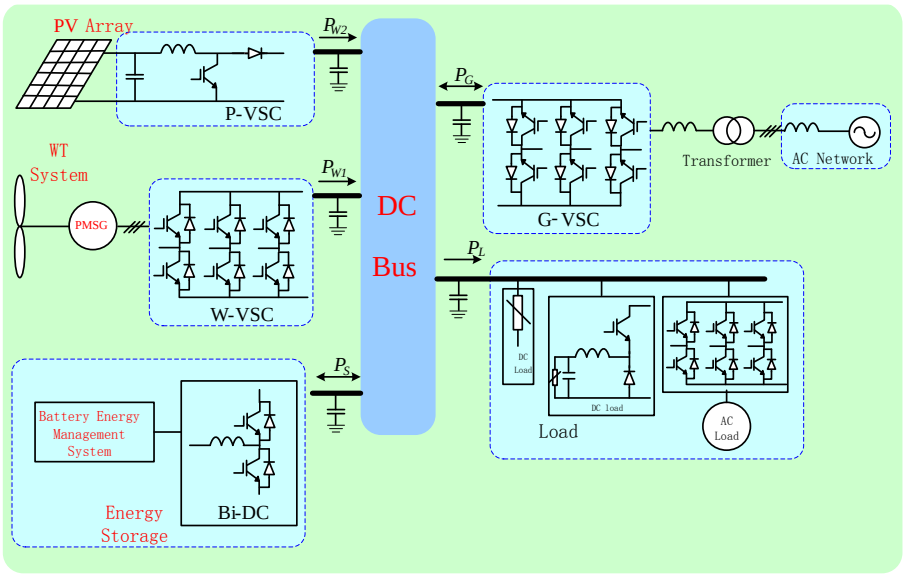


**Figure 1.** DC microgrid configuration.

## 2.2. DC Microgrid Composition

- **Grid-connected converter:** The DC microgrid is integrated with the AC main network through a voltage-sourced Pulse-Width Modulation (PWM) converter Grid-Voltage Sourced Converter (G-VSC). Figure 2 illustrates how G-VSC switches from different operation modes. The parameters for Figure 2 are shown in Table 1. When the DC microgrid operates in a normal grid-connected mode, the DC bus voltage stability is ensured by G-VSC under droop control. However, the G-VSC will switch to current-limiting mode if the interchanged power between the microgrid and the main network reaches the maximum power of G-VSC. When the output power of PV and WT is sufficient, the microgrid will provide power to the main network through G-VSC.

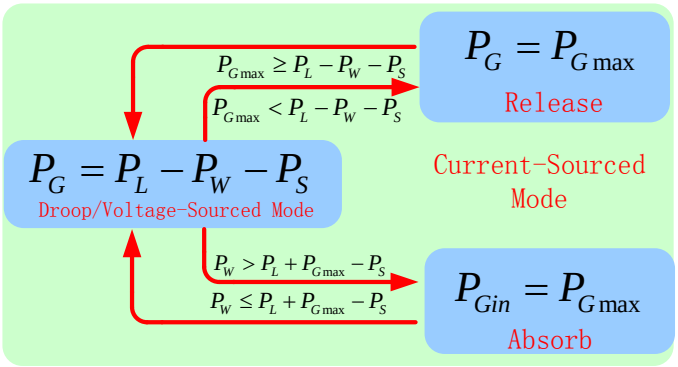


**Figure 2.** Schematic diagram of the AC main network mode-switching.

**Table 1.** Symbols in Figure 2.

| | |
|---|---|
| **PG:** actual output power of AC main network | **SOC:** current state of charge |
| **$PG_{max}$:** the maximum output power of G-VSC | **$SOC_{max}$:** maximum state of charge |
| **$PG_{in}$:** actual absorbed power by AC main network | **$SOC_{min}$:** minimum state of charge |
| **PW:** actual output power of DG unit | **PL:** actual power of loads |
| **$PW_{mppt}$:** maximum tracing power of DG unit | **PN:** rated power of loads |
| **PS:** release(+)/absorb(−) power of battery | **ΔP:** power of shedding loads |
| **$PS_{max}$:** maximum output power of battery | |

- **Distributed generation unit:** The DG unit is composed by the wind turbine generator system and photovoltaic generator system, which are tied with the DC microgrid by a DC/DC converter and a voltage-sourced converter Wind-Voltage Sourced Converter (W-VSC), respectively. In Figure 3, the switching process of the DG unit in different modes is illustrated. In order to capture the most wind and solar energy possible, the DG unit works in the MPPT manner normally, enhancing the energy utilization efficiency. When the wind and solar are sufficient and the DG unit output is large, the DC bus voltage rises, and the operation mode will switch to droop control to sustain the voltage stability. The DG unit will shut down if the main network is not connected, all loads are shed and the battery is fully charged.

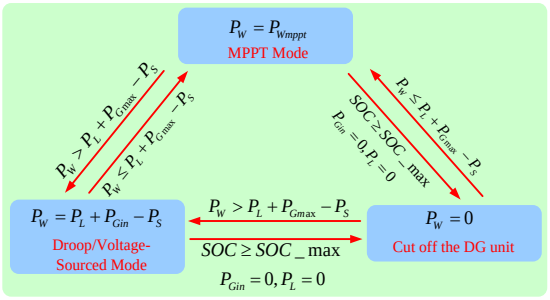


**Figure 3.** Schematic diagram of the DG unit mode-switching.

- **Energy storage battery:** The ES battery is connected with the DC microgrid by a bilateral DC/DC converter and switches its operation modes as in Figure 4. The battery works under the charging mode when the DC microgrid operates normally; when fully charged, the battery would be shed from the microgrid as a standby. However, when the microgrid is islanded due to a main network fault, the ES unit would stabilize the DC bus voltage as a balancing bus, in order to ensure stable system operation.

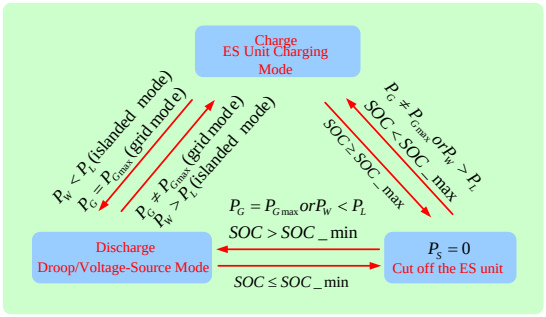


**Figure 4.** Schematic diagram of ES battery mode-switching.

- **Load:** The DC and AC loads are connected with the DC microgrid through a DC/DC converter and DC/AC converter, respectively. The loads unit switches its operation mode as shown in Figure 5. When power supply is insufficient, load-shedding control in terms of loads priority is needed to ensure power balance of the DC microgrid and power supply quality of the important loads.

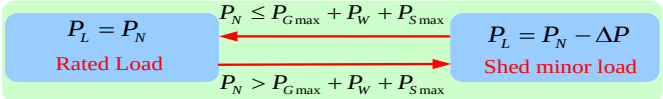


**Figure 5.** Schematic diagram of load mode-switching.

## 3. Research on the Operational Control Strategy of the DC Microgrid

### *3.1. The DC Droop Control Strategy Based on Integrator Current-Sharing*

The traditional DC droop control is presented in Figure 6, in which two distributed power sources in parallel provide power to DC loads. The conventional droop control strategy adopted in Figure 6 is:

$$U_{dci} = U_{dc}^{*} - K_{di} \cdot I_{dci} \tag{1}$$

where $U_{dc}^{*}$ is the no-load voltage of distributed sources and $U_{dci}$ and $I_{dci}$ are the output voltage and current of the distributed source $i$, respectively. $K_{di}$ is the droop coefficient. In Figure 6, $R_{line}1$ and $R_{line}2$ are line resistances of the distributed sources.

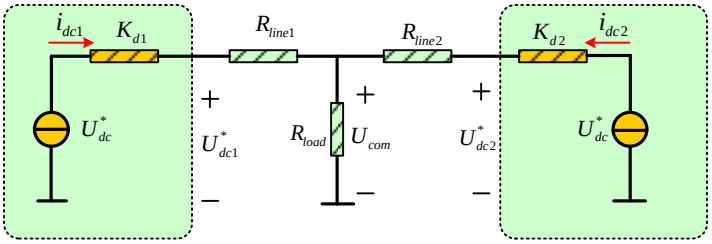


**Figure 6.** Two distributed power sources in parallel based on the conventional droop control.

In order to facilitate the analysis, two distributed power sources are taken as an example to illustrate the power characteristic. The following formulas can be derived from Figure 6:

$$U_{com} = U_{dc}^{*} - K_{d1} \cdot I_{dc1} - R_{line1} \cdot I_{dc1} \tag{2}$$

$$U_{com} = U_{dc}^{*} - K_{d2} \cdot I_{dc2} - R_{line2} \cdot I_{dc2} \tag{3}$$

Combining (2) and (3) yields:

$$\frac{I_{dc1}}{I_{dc2}} = \frac{K_{d2}}{K_{d1}} + \frac{R_{line2} - K_{d2}/K_{d1} \cdot R_{line1}}{K_{d1} + R_{line1}} \tag{4}$$

Generally, the droop coefficient $K_{di}$ is inversely proportional to the nominal power of the DG unit [16]. In (4), it is assumed that two distributed sources have the same capacity for simplifying the analysis, the droop coefficients $K_{d1} = K_{d2}$. Because a difference exists between line parameters of distributed sources:

$$\frac{K_{d2}}{K_{d1}} \neq \frac{R_{line2}}{R_{line1}} \tag{5}$$

the output currents of various distributed sources are different, which causes circulating current.

$$\frac{I_{dc1}}{I_{dc2}} \neq \frac{K_{d1}}{K_{d2}} \tag{6}$$

From the above analysis, the output powers of various converters are different because of the parameter differences of various distributed sources and lines; when it is worse, circulating current arises, which causes distributed sources' output, and system stability is affected. Hence, a DC droop control strategy based on the integrator current-sharing is proposed in this study, and a current-sharing term is employed in the conventional DC droop control strategy:

$$U_{dci} = U_{dc}^{*} - K_{di} \cdot I_{dci} + \Delta U_{dci} \tag{7}$$

In order to achieve power-sharing, the current-sharing term should be constructed as a function of the output power:

$$\Delta U_{dci} = f(P_{dci}) \tag{8}$$

In this paper, with the principle that the integrator can eliminate error, the current-sharing term is constructed as follows:

$$f(P_{dci}) = K_u \cdot \int \left[ (U^*_{com} - U_{com}) - K_{pi} \cdot P_{dci} \right] dt \tag{9}$$

Combining (7)–(9) yields the improved DC droop control strategy based on the integrator current-sharing:

$$U_{dci} = U^*_{dc} - K_{di} \cdot I_{dci} + K_u \cdot \int \left[ (U^*_{com} - U_{com}) - K_{pi} \cdot P_{dci} \right] dt \tag{10}$$

Then, differentiate (11) to get:

$$U^*_{com} = U_{com} + K_{pi} \cdot P_{dci} + \frac{1}{K_u} \cdot \frac{dU_{dci}}{dt} + \frac{K_{di}}{K_u} \cdot \frac{dI_{dci}}{dt} \tag{11}$$

When the system reaches the steady state, the differentials of DC values become zero, then (11) can be expressed as follows:

$$U^*_{com} = U_{com} + K_{pi} \cdot P_{dci} \tag{12}$$

where $U^*_{com}$ is the no-load voltage of the public bus, $U_{com}$ is the actual bus voltage, $K_{pi}$ is the current-sharing coefficient and $K_u$ is the public integrator coefficient. It can be deduced from (12) that:

$$K_{p1} P_{dc1} = K_{p2} P_{dc2} = \ldots\ldots = K_{pi} P_{dci} \tag{13}$$

Therefore, from (13), the current-sharing coefficient can be set in terms of the distributed sources capacity, then the output of distributed sources is rationalized, which avoids circulating current between sources being aroused, affecting system stability. In addition, the $K_u$ coefficient is a global public integrator. $K_u$ is a coefficient related to the integrator changing speed. Since the control method proposed in this paper is a primary-layer control, normally the responding time of the primary-layer is $\Delta t$ = [10 ms, 50 ms], so the integral parameter, calculated by $K_u = 1/\Delta t$, is in the range [20, 100]. Besides, the changing range of the DG output voltage is $\pm$10%, and the nominal power in this paper is set as 380 V, so the maximum changed voltage is 76 V. If the integral parameter $K_u$ is chosen to be 100, then in the time interval $t$ = 10 ms, the voltage is changed by 76 V in the worst situation, which is prone to cause the voltage to cross the border. Taking the above reasons into account, the parameter $K_u$ is set to be 50 in this paper, ensuring the responding speed to be reasonable and the voltage to be maintained in a proper range.

### *3.2. The Hierarchical/Droop Voltage Control Strategy*

For a DC microgrid, constant DC bus voltage means power balance in the system. In order to guarantee the safety and reliability of the system, DC bus voltage should be sustained in a limited range. Assuming the rated voltage of the DC bus is 380 V, the system operation modes can be classified into three types according to DC bus voltage, which is shown in Figure 7. Moreover, the method proposed in this paper is based on the power-sharing of the same kind of DG sources, while for different kinds of DG sources, like PV and WT generation, the hierarchical control method is adopted, in which the control modes of DGs are determined by the common bus voltage.

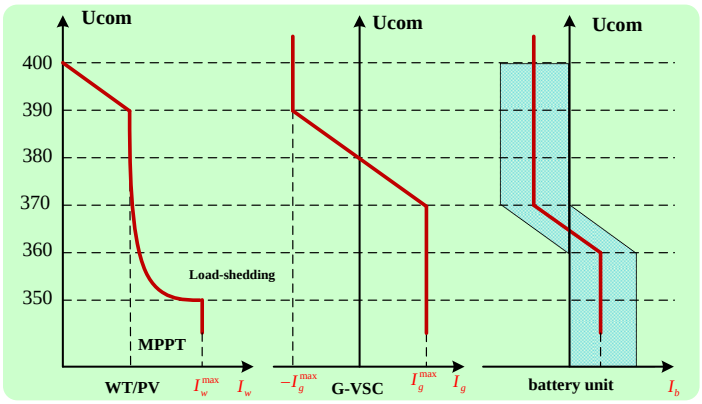


**Figure 7.** Three types of operation modes.

- **Operation Mode 1:** The G-VSC sustains the stability of DC bus voltage; the DG unit operates under the MPPT mode; the storage battery is in constant-current charge under the control of the battery management system and then shed from the microgrid when fully charged. In this mode, the DC bus voltage is maintained within ±10 V of the rated voltage.
- **Operation Mode 2:** The storage battery sustains the stability of the DC bus voltage. When the transmitted power of the AC main network to the DC microgrid reaches the G-VSC limitation, or faults like short-circuit occurred, G-VSC will switch to current-limiting mode. The DG unit operates in the MPPT mode. Under this circumstance, the bus voltage is stabilized within 360 V–370 V.
- **Operation Mode 3:** The DG unit sustains the stability of the DC bus voltage. When the loads are light and the DC bus voltage rises to over 390 V, the battery would charge with the control of the battery management system, and the G-VSC transmits electric power to the AC main network in its maximum power or cut off from the DC microgrid.

The system switches its operation mode as Figure 8 shows. Note that, (1) in order to extend the battery lifetime, discharging in depth is not permitted, which stops discharging when the state of charge (SOC) is reduced under 20%. Meanwhile, overcharging is also not allowed, which makes the battery stop charging when the SOC exceeds 80% [30,31]; (2) When the loads are too heavy that the energy of the DC microgrid is not capable of maintaining the power balance, shedding unimportant loads according to the load priority is needed to sustain the power balance; (3) To avoid frequently switching between different unit work modes, the time delay control is applied in the voltage switch, which means the switching mode is performed only when the voltage is changing continuously in a certain interval.

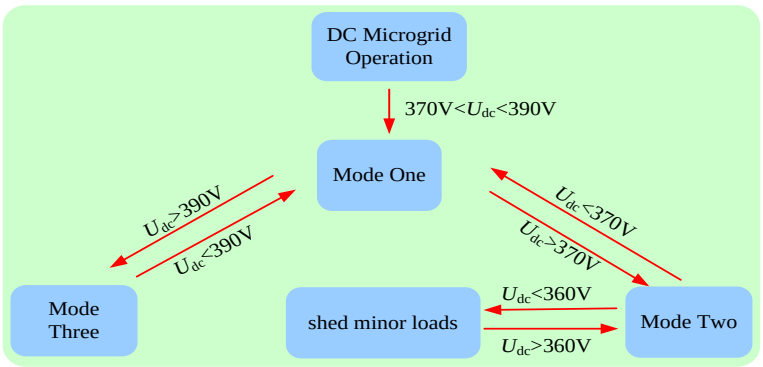


**Figure 8.** Schematic diagram of the system mode-switching.

### 3.3. The Converter Control Scheme of Each Unit

In the local layer control strategy for distributed power sources of the same type, the integrator current-sharing control strategy as Formula (14) proposed in this paper is adopted, and its control block diagram is shown as Figure 9:

$$U_{dci} = U_{dc}^{*} - K_{di} \cdot I_{dci} + K_u \cdot \int \left[ (U_{com}^{*} - U_{com}) - K_{pi} \cdot P_{dci} \right] dt \tag{14}$$

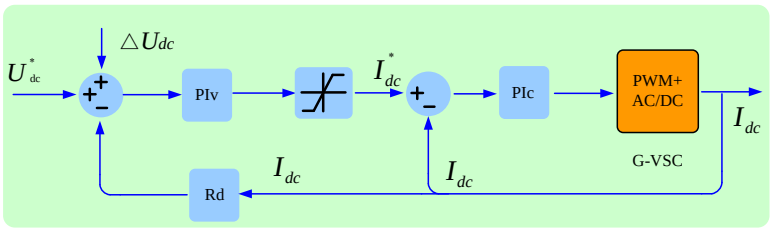


(**a**) Control block diagram of G-VSC

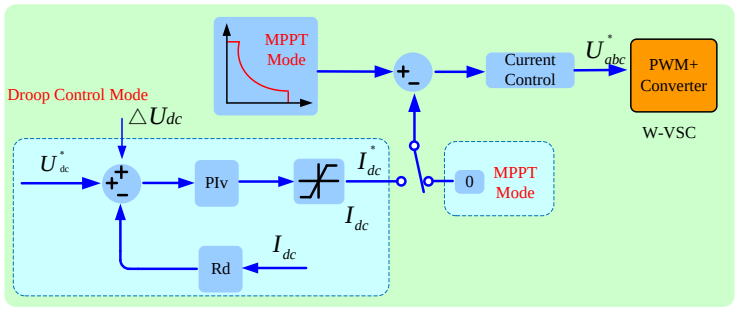


(**b**) Control block diagram of the DG unit

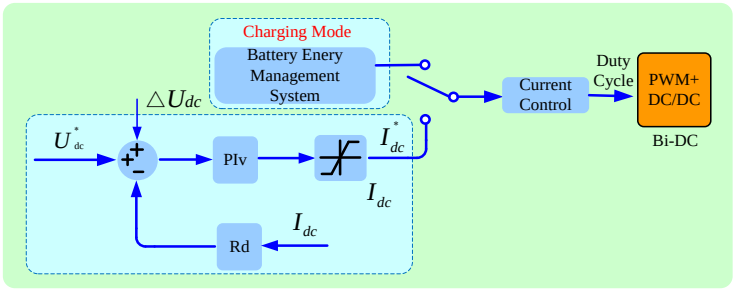


(**c**) Control block diagram of the battery Bi-DC

**Figure 9.** Control block diagram of the converters.

Additionally, in the coordinated control of the system layer, the improved hierarchical/droop control strategy based on the DC bus voltage introduced in this paper is employed, so as to ensure the power flow balance of the microgrid in different hierarchical zones. The operational modes are shown in Figure 8.

According to the load priority, loads can be sorted into n levels: Level-1, Level-2, Level-3, . . . , Level-n, and the level is greater as the value of n is smaller. Loads in n different levels all have the corresponding cut-off time, and T1 > T2 > T3, . . . , > Tn. When the bus voltage is detected below 360 V, all timers start. If the timer of Level-n reaches Tn, then the loads of Level-n are shed immediately. After load-shedding, T1, T2, T3, . . . , T(n − 1) will be cleared if the DC bus voltage returns to normal, while the loads in Level-(n − 1) will be cut off if the voltage is still under 360 V and it continues to T(n − 1). The rest can be done in the same manner. The load-shedding process is shown in Figure 10.

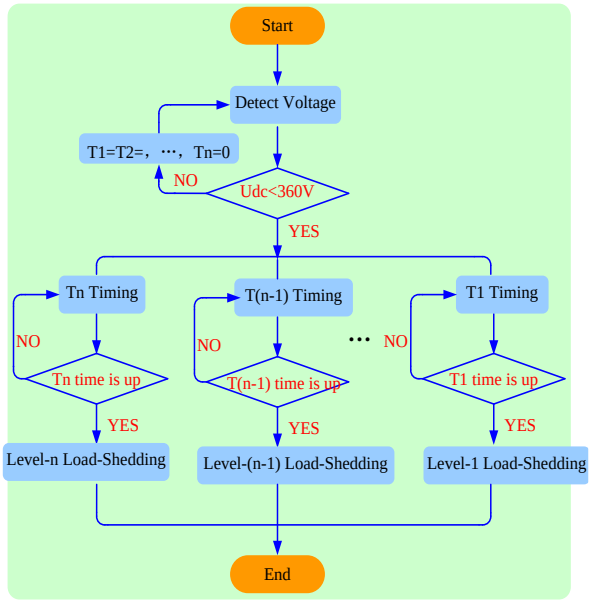


**Figure 10.** Schematic diagram of the load-shedding process.

## 4. Simulation Results

### *4.1. Verification to the Droop Control Strategy Based on Integrator Current-Sharing*

In order to verify the feasibility of the droop control strategy based on integrator current-sharing proposed in this study, the simulation model of the microgrid is constructed using the MATLAB/Simulink software. The simulation system of the DC microgrid is composed of three distributed power sources with the same capacity and common loads. Because of the difference existing in different feeder parameters of distributed sources, the feeders of the three DG units are assumed to be 0.5 km, 2 km and 5 km, respectively, and the DC common load as 13.5 kW. The distributed micro-source parameters under the droop control based on integrator current-sharing are listed in Table 2.

**Table 2.** The control parameter of DG units.

| Parameter | Value | Parameter | Value |
|---|---|---|---|
| $U^*_{com}$ (V) | 380 | $U^*_{dc}$ (V) | 380 |
| $K_d$ | 0.2 | $K_{p1}$ | 0.004 |
| $R_{line1}$ (Ω) | 0.05 | $K_{p2}$ | 0.004 |
| $R_{line2}$ (Ω | 0.2 | $K_{p3}$ | 0.004 |
| $R_{line3}$ (Ω) | 0.5 | $K_{u1}$ | 50 |
| $K_{u2}$ | 50 | $K_{u3}$ | 50 |

With the control method proposed in this paper, three DG units with the capacity of 10 kW are connected to the bus in parallel. The simulation result is shown as Figure 11. In order to facilitate the contrast, in the initial phase $t$ = [0 s, 1.0 s], the conventional droop control strategy is adopted, while in the interval $t$ = [1.0 s, 2.0 s], the droop control strategy based on integrator current-sharing proposed in this study is employed.

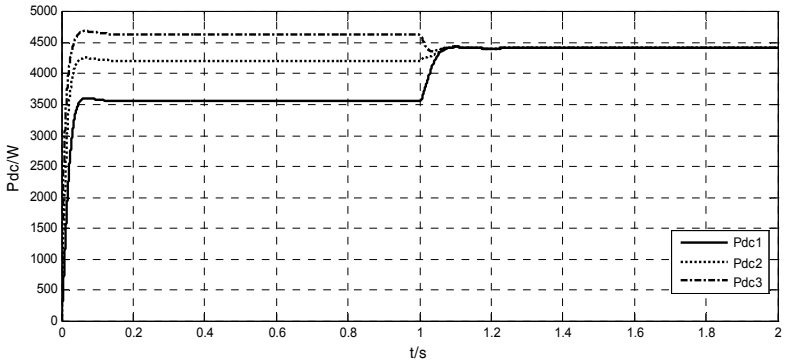


(**a**) DG output powers under the conventional and proposed control strategy

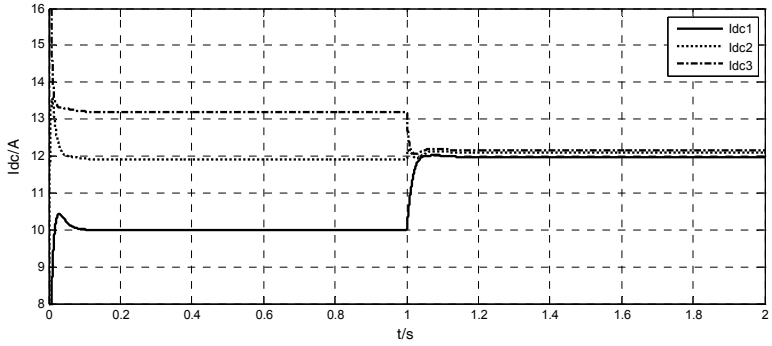


(**b**) DG output currents under the conventional and proposed control strategy

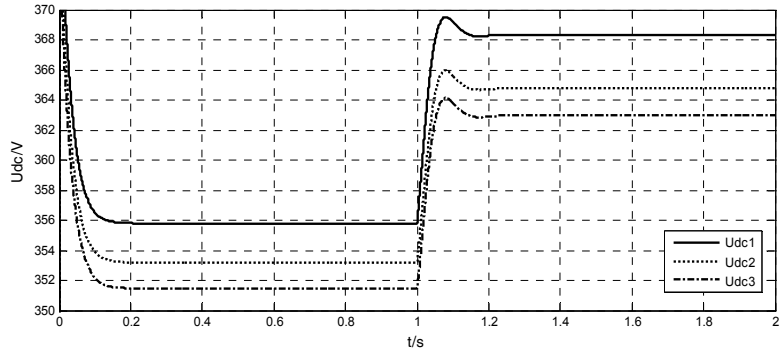


(**c**) DG output voltages under the conventional and proposed control strategy

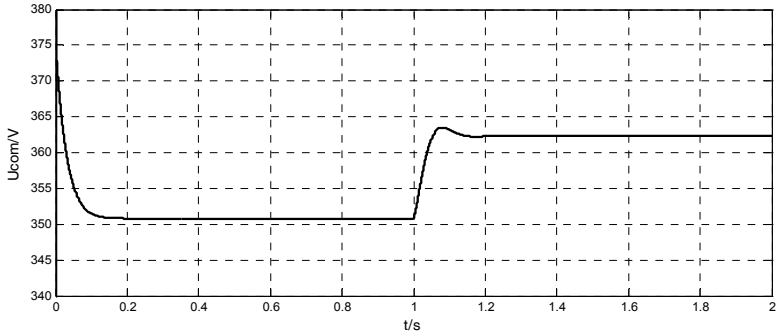


(**d**) DC bus voltage under the conventional and proposed control strategy

**Figure 11.** Simulation results of the conventional and proposed control strategy.

Figure 11a,b presents the power and current waves of DGs under the conventional and improved control, respectively. From the figures, before $t$ = 1.0 s, large deviation exits both in the output power and current of DG units under the conventional control due to the differences among different feeder

resistances. The output power difference between DG1 and DG3 is 1000 W. After $t$ = 1.0 s, the output steady-state currents of the DG units with the same capacity are almost the same, and the output powers are exactly the same; the circulating current is nearly zero. Figure 11c,d displays the output voltage and public bus voltage of the DG units under conventional and improved control, respectively. Under the conventional control strategy, the output voltages of different DG units are 356 V, 353 V and 351.5 V, respectively. The output voltage is relatively low because of the droop control strategy, which affects the system voltage level. However, after $t$ = 1.0 s, the current-sharing term constructed in the new method not only achieves power-sharing, but also improves the system voltage by 10 V. Moreover, the public bus voltage is improved to some extent, enhancing the system voltage stability on the whole.

In conclusion, the proposed droop control strategy based on integrator current-sharing not only can realize power-sharing, which avoids circulating current and makes the DG unit capability come into full play, but it also enhances the voltage level and stability of the system. Therefore, this case can fully justify the feasibility and effectiveness of the proposed method.

In addition, the method proposed in this paper is that no communication is needed between different DG sources, and the current-sharing control is achieved only by the common bus voltage signal. The communication between different DGs will disable the microgrid be a plug-and-play solution, while the microgrid in this paper remains to have a plug-and-play characteristic.

### *4.2. Verification to System Coordinated Control Strategy*

In order to verify the effectiveness of the hierarchical/droop voltage control strategy, the simulation model shown in Figure 1 is built in MATLAB/Simulink, and the system is configured as shown in Table 3. According to the above analysis of the three operation modes, three responding simulation tests are conducted. In addition, the constant illumination model is adopted for PV, and the constant wind speed model is adopted for wind generation. When switching modes, we assume the illumination and wind speed are under step changes. Furthermore, the constant power load and lead-acid battery are used in this work. In the case that the battery discharges too deeply and affects its lifetime, the Depth of Discharge (DoD) is chosen as 60% in this paper, effectively prolonging the battery lifetime.

**Table 3.** Configuration of the DC microgrid.

| | |
|---|---|
| Rated DC bus voltage | 380 V |
| Maximum output power of the AC main network | 10 kW |
| Maximum output power of W-VSC in the WT generation system | 5 kW |
| Maximum output power of DC/DC in the PV generation system | 10 kW |
| Maximum output power of Bi-DC in the ES system | 5 kW |
| Load 1 (Level1) | 10 kW |
| Load 2 (Level2) | 5 kW |
| Load 3 (Level3) | 5 kW |

- **Simulation 1:** The system stably operates in Mode 1, and the AC main network is working to maintain the stability of the DC bus voltage. The result is depicted in Figure 12, and Table 4 shows the major incidents in the first simulation. From Figure 12, when the load and DG unit output power have changed, G-VSC adjusts the exchange power between the DC microgrid and the main network according to the droop characteristic to sustain the bus voltage within 370 V–390 V, while the battery is cut off from the DC bus, becoming a standby.

**Table 4.** Major incidents in Simulation 1.

| Incident | Operation Condition | Time (s) |
|---|---|---|
| 1 | Battery charges by linking with the DC bus | 0.4 |
| 2 | The output of WT generation system increases from 3 kW–4.5 kW | 1.0 |
| 3 | Load 2 is connected to the DC bus | 2.0 |
| 4 | Battery is cut off from the DC bus after being fully charged | 2.5 |
| 5 | The output of the PV generation system rises from 5 kW–8 kW | 3.0 |
| 6 | Load 3 is connected to the DC bus | 4.0 |
| 7 | Load 3 is shed from the DC bus | 4.5 |

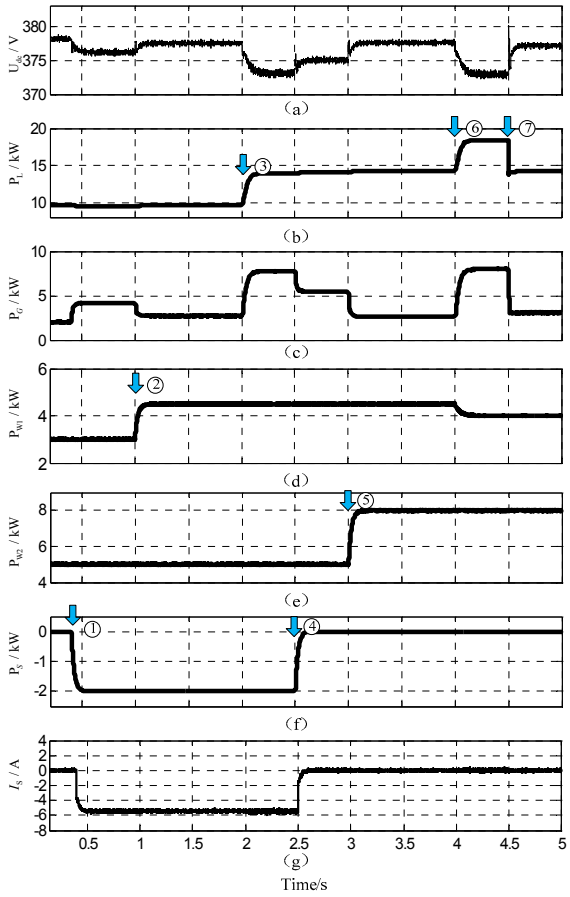


**Figure 12.** Simulation waves of Simulation 1: (**a**) DC bus voltage; (**b**) load power; (**c**) output power of G-VSC; (**d**) output power of the WT generation system; (**e**) output power of the PV generation system; (**f**) power released(+)/absorbed(−) of the battery; (**g**) discharging(+)/charging(−) the current of the battery.

- **Simulation 2:** When the battery works to maintain the stability of the DC bus voltage, the simulation result is shown as Figure 13, while Table 5 lists the major incidents in the simulation. At first, the system stably runs in Mode 1. At $t$ = 1.0 s, the AC main network malfunctions and is shed from the DC microgrid, after which the system switches to Mode 2 in which the battery works to sustain the stability of the DC bus voltage. At $t$ = 1.2 s, the fault is removed and the system returns to operation Mode 1. Load 3 and Load 2 are tied with the DC bus at $t$ = 2.0 s and $t$ = 3.0 s, respectively. This causes the output power of the AC main network to gradually attain the maximum power allowance of G-VSC and then turn into current-limiting mode, where the system switches back to Mode 2 again. Although the loads and micro-sources' output still change afterwards, the DC bus voltage is maintained within 360 V–370 V through the droop control of

the storage battery. At $t$ = 4.7 s, the output power cannot meet the load demand since the output of the PV generation system has been reduced. According to the load grades, Load 3 is cut off. After cutting, the output power can meet the load requirement, and the system can stably operate in the mode.

**Table 5.** Major incidents in Simulation 2.

| Incident | Operation Conditions | Time (s) |
|---|---|---|
| 1 | AC main network fails | 1.0 |
| 2 | AC main network recovers from the failure | 1.2 |
| 3 | Load 3 is connected to the DC bus | 2.0 |
| 4 | Load 2 is connected to the DC bus | 3.0 |
| 5 | The output of the WT generation system decreases from 3 kW–1 kW | 4.0 |
| 6 | The output of the PV generation system reduces from 5 kW–3 kW | 4.5 |
| 7 | Load 3 is shed from the DC bus | 4.7 |

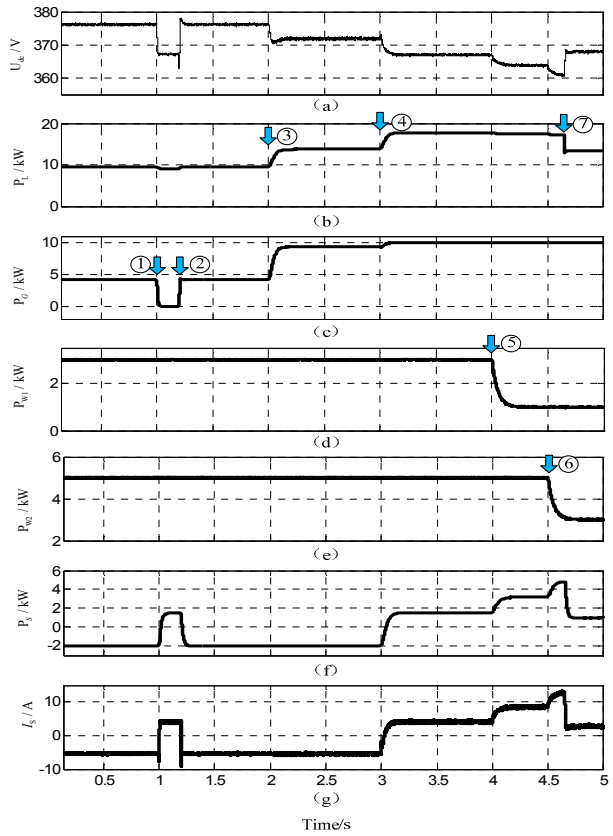


**Figure 13.** Simulation waves of Simulation 2: (**a**) DC bus voltage; (**b**) load power; (**c**) output power of G-VSC; (**d**) output power of the WT generation system; (**e**) output power of the PV generation system; (**f**) power released(+)/absorbed(−) of the battery; (**g**) discharging(+)/charging(−) current of the battery.

- **Simulation 3:** When the islanded mode is taken into consideration and the DG unit sustains the stability of the DC bus voltage, the simulation result is shown as Figure 14. Table 6 lists the major incidents in the simulation. At $t$ = 1 s, the DC microgrid in the islanded mode is disconnected from the main network, causing the system to switch to operation Mode 2, in which the battery maintains the stability of the DC bus voltage. At $t$ = 2 s, the output power of the DG unit increases, and the DC bus voltage rises over 390 V, after which the DC microgrid switches to Mode 3. In Mode 3, the DG generation unit is under voltage-sourced control to sustain the stability of

the DC bus voltage and the power balance. The output of the PV and WT generation systems is decided in terms of their capacity ratio (2:1). At $t$ = 3 s, the active load changes, the stability of the DC bus voltage and system power balance are achieved through the droop control of the DG unit. At $t$ = 4 s, the battery is fully charged and cut off from the DC microgrid.

**Table 6.** Major incidents in Simulation 3.

| Incident | Operation conditions | Time(s) |
|---|---|---|
| 1 | DC microgrid disconnected from the main network, in islanded mode | 1.0 |
| 2 | The output of the DG generation system increases dramatically | 2.0 |
| 3 | Load 1 is shed from the DC bus<br>Load 2 is connected to the DC bus | 3.0 |
| 4 | Battery is cut off from the DC bus after being fully charged | 4.0 |

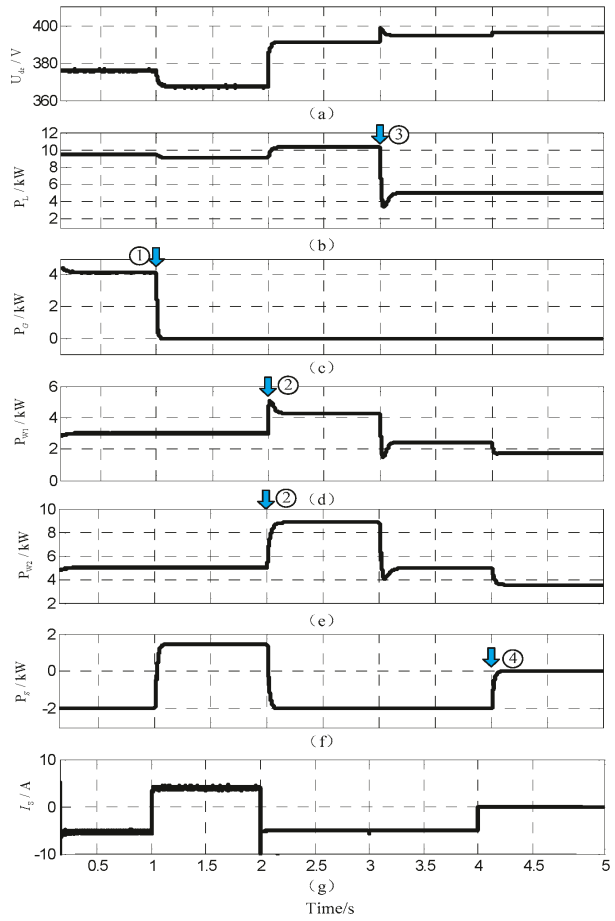


**Figure 14.** Simulation waves of Simulation 3: (**a**) DC bus voltage; (**b**) load power; (**c**) output power of G-VSC; (**d**) output power of the WT generation system; (**e**) output power of the PV generation system; (**f**) power released(+)/absorbed(−) of the battery; (**g**) discharging(+)/charging(−) current of the battery.

### *4.3. Verification to the Actual PV and WT Generation System*

In order to verify the voltage stability of actual PV and WT generation in the DC microgrid, actual data of PV and WT generation are used in this case. The DC microgrid system operates in Mode 1. In the Figure 15, in the time interval $t$ = [1.5 s, 2 s], the PV gets the maximum illumination, with an output of 5 kW or so, while the output of WT generation is stochastic, changing within

[3 kW, 5.8 kW]. The rest of the demanded power is provided to the load by the grid-connected inverter G-VSC, ensuring the common bus voltage within in a certain range, which verifies the stability of the DC microgrid voltage.

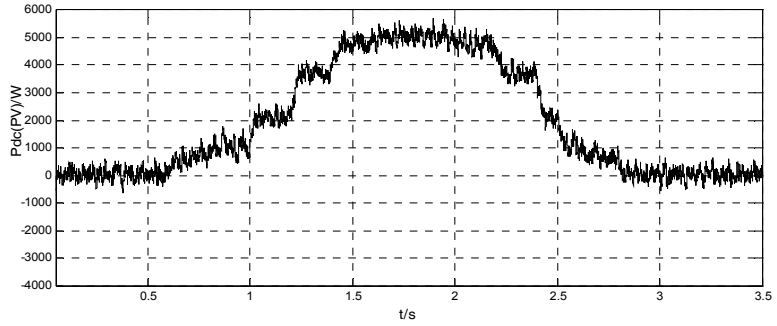


(**a**) Output power of the PV generation system

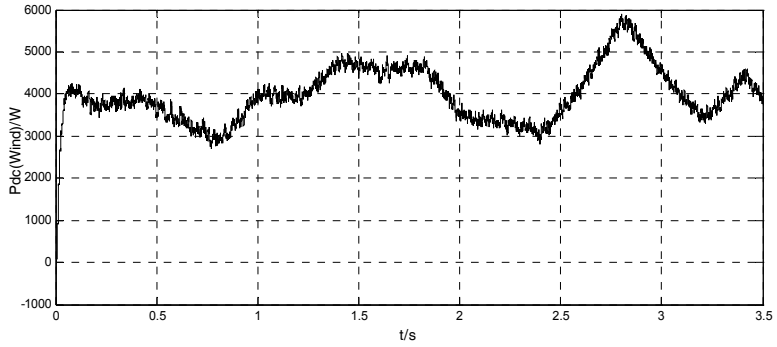


(**b**) Output power of the WT generation system

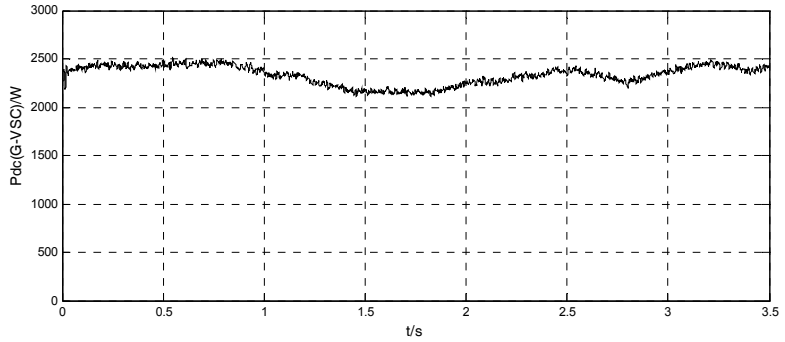


(**c**) Output power of G-VSC

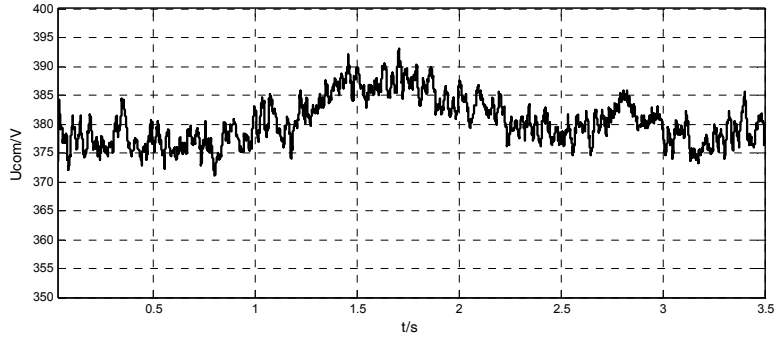


(**d**) DC bus voltage

**Figure 15.** Simulation results of the conventional and proposed control strategy.

## 5. Conclusions

Taking a PV/WT/ES DC microgrid applied to small-sized commercial and residential buildings as a paradigm, this paper proposes a hierarchical/droop voltage control strategy based on the DC bus voltage, which controls the operation mode of the DC microgrid by detecting the change of the bus voltage to sustain the power balance of the DC microgrid. In addition, in order to avoid the drawbacks of the conventional droop control, an improved DC droop control strategy based on integrator current-sharing is introduced. Simulation results verify the effectiveness and feasibility of the proposed scheme. Through the analysis, the following conclusion can be made: (1) with the help of the integral term, the improved droop control strategy can achieve power-sharing, as well as improve the DC bus voltage; (2) in the method proposed in this paper, judging by using the common DC voltage can make the operation modes switch smoothly, ensuring that the DG sources are working at their maximum efficiency, and the system has transient steady characteristic; (3) the strategy only detects local information of various units, so there is no communication between different DG sources, thereby improving the flexibility and reliability of the control and meaning that the DC microgrid system can be a plug-and-play solution.

**Author Contributions:** The paper was a collaborative effort between the authors. The authors contributed collectively to the theoretical analysis, modeling, simulation, and manuscript preparation.

**Conflicts of Interest:** The authors declare no conflict of interest.

## References

1. Yan, B.; Wang, B.; Zhu, L. A novel, stable, and economic power sharing scheme for an autonomous microgrid in the energy internet. *Energies* **2015**, *8*, 12741–12764. [CrossRef]
2. Lim, Y.; Kim, H.M.; Kinoshita, T. Distributed load-shedding system for agent-based autonomous microgrid operations. *Energies* **2014**, *7*, 385–401. [CrossRef]
3. Lasseter, R.H.; Paigi, P. Microgrid: A conceptual solution. In Proceedings of the IEEE Conference on Power Electronics Specialists, Aachen, Germany, 20–25 June 2004; pp. 4285–4290.
4. Patterson, M.; Macia, N.F.; Kannan, A.M. Hybrid microgrid model based on solar photovoltaic battery fuel cell system for intermittent load applications. *IEEE Trans. Energy Convers.* **2015**, *30*, 359–366. [CrossRef]
5. Xiao, H.; Luo, A.; Shuai, Z. An Improved control method for multiple bidirectional power converters in hybrid AC/DC microgrid. *IEEE Trans. Smart Grid* **2016**, *7*, 340–347. [CrossRef]
6. Salomonsson, D.; Sannino, A. A low-voltage DC distribution system for commercial power systems with sensitive electronic loads. *IEEE Trans. Power Deliv.* **2007**, *22*, 1620–1627. [CrossRef]
7. Mehrdad, B.; Abolfazl, J.; Mehdi, E. Cooperative energy management of hybrid DC renewable grid using decentralized control strategies. *Energies* **2016**, *9*, 859.
8. Liu, Y.Q.; Wang, J.Z.; Li, N.N.; Fu, Y.; Ji, Y.C. Enhanced load power sharing accuracy in droop-controlled DC microgrids with both mesh and radial configurations. *Energies* **2015**, *8*, 3591–3605. [CrossRef]
9. Gao, F.; Bozhko, S.; Costabeber, A. Comparative stability analysis of droop control approaches in voltage-source-converter-based DC microgrids. *IEEE Trans. Power Electron.* **2017**, *32*, 2395–2415. [CrossRef]
10. Vu, T.V.; Paran, S.; Diaz, F. An alternative distributed control architecture for improvement in the transient response of DC microgrids. *IEEE Trans. Ind. Electron.* **2016**, *64*, 574–584. [CrossRef]
11. Hamzeh, M.; Ghazanfari, A.; Mohamed, Y. Modeling and design of an oscillatory current-sharing control strategy in DC microgrids. *IEEE Trans. Ind. Electron.* **2015**, *62*, 6647–6657. [CrossRef]
12. Bryan, J.; Duke, R.; Round, S. Decentralized generator scheduling in a nanogrid using DC bus signaling. In Proceedings of the IEEE Power Engineering Society General Meeting, Denver, CO, USA, 6–10 June 2004; pp. 977–982.
13. Khorsandi, A.; Ashourloo, M.; Mokhtari, H. Automatic droop control for a low voltage DC microgrid. *IET Gener. Trans. Distrib.* **2016**, *10*, 41–47. [CrossRef]
14. Lu, X.; Wan, J. Modeling and Control of the Distributed Power Converters in a Standalone DC Microgrid. *Energies* **2016**, *9*, 217. [CrossRef]

15. Dou, C.; Yue, D.; Guerrero, J.M. Multiagent System-Based Distributed Coordinated Control for Radial DC Microgrid Considering Transmission Time Delays. *IEEE Trans. Smart Grid* **2016**, *99*, 1–12. [CrossRef]
16. Hu, R.; Weaver, W.W. DC microgrid droop control based on battery state of charge balancing. In Proceedings of the IEEE Power and Energy Conference, Urbana, IL, USA, 19–20 February 2016; pp. 1–8.
17. Hwang, C.S.; Kim, E.S.; Kim, Y.S. A Decentralized Control Method for Distributed Generations in an Islanded DC Microgrid Considering Voltage Drop Compensation and Durable State of Charge. *Energies* **2016**, *9*, 1070. [CrossRef]
18. Salomonsson, D.; Soder, L.; Sannino, A. An adaptive control system for a dc microgrid for data centers. *IEEE Trans. Ind. Appl.* **2008**, *44*, 1910–1917. [CrossRef]
19. Xu, L.; Chen, D. Control and operation of a DC microgrid with variable generation and energy storage. *IEEE Trans. Power Deliv.* **2011**, *26*, 2513–2522. [CrossRef]
20. Zhou, T.; Francois, B. Energy management and power control of a hybrid active wind generator for distributed power generation and grid integrator. *IEEE Trans. Ind. Electron.* **2011**, *58*, 95–104. [CrossRef]
21. Guerrero, J.M.; Vasquez, J.C.; Matas, J. Hierarchical control of droop-controlled AC and DC Microgrids—A general approach toward standardization. *IEEE Trans. Ind. Electron.* **2011**, *58*, 158–172. [CrossRef]
22. Chen, D.; Xu, L. Autonomous DC voltage control of a DC microgrid with multiple slack terminals. *IEEE Trans. Power Syst.* **2012**, *27*, 1897–1905. [CrossRef]
23. Han, Y.; Chen, W.R.; Li, Q. Energy management strategy based on multiple operating states for a photovoltaic/fuel cell/energy storage DC microgrid. *Energies* **2017**, *10*, 136. [CrossRef]
24. Teleke, S.; Baran, M.E.; Huang, A.Q.; Bhattacharya, S.; Anderson, L. Control strategies for battery energy storage for wind farm dispatching. *IEEE Trans. Energy Convers.* **2009**, *24*, 725–732. [CrossRef]
25. Dragicevic, T.; Guerrero, J.M.; Vasquez, J.C. Supervisory control of an adaptive-droop regulated DC microgrid with battery management capability. *IEEE Trans. Power Electron.* **2013**, *29*, 1–12. [CrossRef]
26. Lu, X.; Guerrero, J.M.; Sun, K. An improved droop control method for DC microgrids based on low bandwidth communication with DC bus voltage restoration and enhanced current sharing accuracy. *IEEE Trans. Power Electron.* **2013**, *29*, 1–12. [CrossRef]
27. Lee, S.W.; Cho, B.H. Master–slave based hierarchical control for a small power DC-distributed microgrid system with a storage device. *Energies* **2016**, *9*, 880. [CrossRef]
28. Wang, P.B.; Lu, X.N.; Yang, X. An improved distributed secondary control method for DC microgrids with enhanced dynamic current sharing performance. *IEEE Trans. Power Electron.* **2016**, *31*, 6658–6673. [CrossRef]
29. Dragicevic, T.; Lu, X.N.; Vasquez, J.C. DC Microgrids—Part I: A review of control strategies and stabilization techniques. *IEEE Trans. Power Electron.* **2016**, *31*, 4876–4891. [CrossRef]
30. Yu, S.Y.; Kim, H.J.; Kim, J.H. SoC-Based Output Voltage Control for BESS with a Lithium-Ion Battery in a Stand-Alone DC Microgrid. *Energies* **2016**, *9*, 924. [CrossRef]
31. Lu, X.; Sun, K.; Guerrero, J.M. SoC-based droop method for distributed energy storage in DC microgrid applications. In Proceedings of the 2012 IEEE International Symposium on Industrial Electronics (ISIE), Hangzhou, China, 28–31 May 2012; pp. 1640–1645.